Effects of turbulence and heterogeneous emissions on photochemically active species in the convective boundary layer

Maarten C. Krol and M. Jeroen Molemaker

Institute for Marine and Atmospheric Research Utrecht, Utrecht, Netherlands

Jordi Vilà Guerau de Arellano

Department of Meteorology and Air Quality, Wageningen University, Wageningen, Netherlands

Abstract. Photochemistry is studied in a convective atmospheric boundary layer. The essential reactions that account for the ozone formation and depletion are included in the chemical mechanism which, as a consequence, contains a wide range of timescales. The turbulent reacting flow is modeled with a large-eddy simulation (LES) code. The deviations from chemical equilibrium that are caused by turbulent motions are investigated in terms of the intensity of segregation. For the studied cases it is found that the volume-averaged concentrations calculated with the LES code agree well with the concentrations calculated with a box model. The reaction rate between RH (a generic hydrocarbon emitted at the surface) and OH is most strongly affected (3% slower than in the box model). However, if RH is emitted nonuniformly at the surface, or if the RH–OH reaction rate is increased, the volume-averaged RH destruction by OH may be slowed down by as much as 30% compared to a box model. Sensitivity studies showed that the intensity of segregation between RH and OH not only depends on the strength and spatial distribution of the RH emissions but also on the way NO is emitted in the model atmosphere. The results obtained indicate that the assumption that localized emissions of reactive hydrocarbons, for example, isoprene or terpenes, are instantaneously mixed may lead to an underestimation of their atmospheric lifetime.

1. Introduction

Transport and mixing play a key role in the chemistry of the atmosphere [e.g., *Kley*, 1997]. The atmospheric residence time of many compounds is not only determined by chemical factors but also by atmospheric processes, such as mixing. In the atmospheric boundary layer (ABL), species like nonmethane hydrocarbons (NMHCs) and nitrogen oxides have a chemical lifetime that ranges from less than minutes to days. If the chemical lifetime is short, the interaction between chemical production/destruction and mixing processes is expected on the spatial scales of the ABL [*Vilà-Guerau de Arellano and Lelieveld*, 1998]. For instance, the reaction between ozone (O_3) and nitrogen oxide (NO) has a typical timescale of a few minutes, which is of the same order as the characteristic mixing time of the convective boundary layer.

The ABL constitutes an important part of the atmosphere since almost all natural and anthropogenically produced chemicals are emitted in this layer. The efficiency of mixing in the ABL is highly variable and depends strongly on the heat flux at the Earth's surface. Turbulence is enhanced when the surface is heated by the Sun during daytime. A convective layer develops in which emitted species are quickly transported upwards to higher atmospheric levels. The turbulent structure of the convective boundary layer (CBL) is characterized by thermal updrafts surrounded by slower subsiding motions. The timescale of these motions is typically 15 min and a typical height of the CBL ranges between 1000 and 2000 m. When a chemically reactive species is transported by these turbulent motions, its concentration in the updraft may differ from the downdraft concentration. Species that are entrained from the free troposphere may be segregated from species that are emitted at the surface. As a consequence of this incomplete mixing, chemical transformations may proceed at a slower rate [*Moeng and Wyngaard*, 1984; *Schumann*, 1989].

In the CBL, numerical studies have mostly been restricted to the generic reaction between two species A and B [*Schumann*, 1989; *Sykes et al.*, 1994; *Molemaker and Vilà-Guerau de Arellano*, 1998]. The species are injected in the model domain at the surface or are entrained from the overlying free troposphere. Due to the fully developed three-dimensional turbulence in the CBL, large-eddy simulation (LES) models can be employed to simulate the flow field which advects the chemical species. Alternatively, one-dimensional (1-D) second-order closure and mass flux models have been formulated [*Verver et al.*, 1997; *Petersen et al.*, 1999]. These studies all show that a reaction between two species in the CBL is retarded when the timescale of the chemical reaction is of the same order or faster than the transport timescale.

In this paper we go one step beyond the simple second-order irreversible reaction in the CBL. We investigate how the characteristics of the CBL influence the chemical transformations that are representative for daytime photochemistry. A three-dimensional model is used to simulate atmospheric chemistry in convective turbulence. The chemical scheme simulates the chemical formation of ozone under the influence of ultraviolet radiation in the presence of NO_x ($= NO + NO_2$) and hydrocarbons. More specifically, the following questions will be addressed.

1. How do turbulent motions in the CBL affect complex photochemical transformations which are characterized by a wide range of chemical timescales? How do the volume-averaged chemical transformations (calculated with the LES model) compare to the transformations calculated with a box model?

2. What are the effects on the chemical transformations when the reactive species are not emitted uniformly, but with a nonuniform spatial distribution instead?

These questions are fundamental for the large-scale modeling of atmospheric chemistry. Global or regional scale models (horizontal resolution of 10—1000 km) do not resolve the turbulence in the CBL nor strongly localized emissions. Usually, very crude descriptions of the boundary layer turbulence are implemented in such models [*Peters et al.*, 1995]. Examples of localized emissions are the release of reactive hydrocarbons by forests and NO_x emissions by anthropogenic sources, which can significantly contribute to ozone formation upon mixing. The results presented here (horizontal resolution $\approx$ 50 m) therefore give an indication of the errors that are associated with larger-scale models and may be used to develop and validate parameterizations.

A previous study [*Gao and Wesely*, 1994] coupled a complex chemical mechanism to a second-order closure 1-D model in a neutral ABL. In contrast to our work, the horizontal distribution of trace species was not explicitly taken into account in that study. Here for the first time we present results from a photochemistry scheme that has been coupled to a large-eddy simulation model.

2. Simulation Description

2.1. Photochemistry

Table 1 lists the photochemistry scheme that will be studied in the CBL. A similar scheme has been studied by *Krol and Poppe* [1998] who showed that the scheme contains the essential nonlinear features that are also present in more complex photochemical models. The conclusions that are derived from this simplified chemical scheme cannot be extended to large-scale models. However, the results reveal for which conditions large effects of the turbulence on the chemical transformations are expected. A key aspect of this study is that the chemical scheme contains a wide range of chemical timescales (i.e., from seconds to weeks). We focus primarily on departures from the chemical equilibrium that are caused by turbulent motions.

Since we are mainly interested in the influence of turbulence on the chemical transformation in the CBL, we make the important assumption that the photolysis rates and reaction rates are constant in the entire domain. This assumption enables a straightforward comparison with box model results that are obtained with the same set of rate constants. The atmospheric conditions that are prescribed are typical for a continental boundary layer during summer. The number density of air is taken as 2.5×10^{19} cm^{-3} and the reaction rates are calculated at 298 K. Water vapor, which is important for OH radical formation after ozone photolysis, is present at a relative humidity of 45%. Photolysis rates are calculated for 45° latitude at midday summer solstice.

The chemistry scheme contains six reactive species (O_3, NO, NO_2, RH, HO_2, OH); species which are taken constant (H_2O, M ($= O_2 + N_2$), CO); and species that are assumed to be end-products (HNO_3, H_2O_2). These latter species are not influencing the variable species.

OH is characterized by a very short timescale. This means that the chemical terms in the OH conservation equation are much larger than the advection and diffusion terms which implies that within a grid box much more OH is produced and destroyed than is advected. Production and destruction of OH is determined by the longer-lived species and, consequently, its concentration can be calculated from

$$OH = \frac{2J_1O_3 + k_3HO_2NO + k_4HO_2O_3}{k_2(CO + fRH) + k_6NO_2 + k_7O_3 + k_8HO_2}. \quad (1)$$

A similar steady state approximation is applied for the short-lived oxygen radicals that are formed after O_3 and NO_2 photolysis. These radicals are therefore not included in Table 1.

Table 1. Photochemical Reaction Scheme

Parameter	Value	Consumed		Produced
J_1^*	2.7×10^{-6}	O_3	$\xrightarrow{H_2O}$	$2\ OH + O_2$
J_2	8.9×10^{-3}	NO_2	$\xrightarrow{O_2}$	$NO + O_3$
k_1	4.75×10^{-4}	$O_3 + NO$	$\longrightarrow$	$NO_2 + O_2$
k_2	6.0×10^{-3}	$OH + CO$	$\xrightarrow{O_2}$	$HO_2 + CO_2$
$k_2 \times f$	$6.0 \times 10^{-3} \times f$	$OH + RH$	$\longrightarrow$	$HO_2 + products$
k_3	2.1×10^{-1}	$HO_2 + NO$	$\longrightarrow$	$OH + NO_2$
k_4	5.0×10^{-5}	$HO_2 + O_3$	$\longrightarrow$	$OH + 2\ O_2$
k_5	7.25×10^{-2}	$2\ HO_2$	$\longrightarrow$	$H_2O_2 + O_2$
k_6	2.75×10^{-1}	$OH + NO_2$	$\longrightarrow$	HNO_3
k_7	1.75×10^{-3}	$OH + O_3$	$\longrightarrow$	$HO_2 + O_2$
k_8	2.75	$OH + HO_2$	$\longrightarrow$	$H_2O + O_2$

All reaction rate constants are taken from *Stockwell et al.* [1990] (see also *Poppe and Lustfeld* [1996]). Photolysis frequencies are given in s^{-1}. Reaction rates are given in $ppb^{-1}\ s^{-1}$. The factor f that appears in the reaction rate of $RH + OH$ is variable and ranges from 100 to 300. Initially, f is set to 100.
$^*J_1$ is the product of the photolysis frequency for $O_3 + h\nu \rightarrow O(^1D) + O_2$ multiplied by the yield of the reaction $O(^1D) + H_2O$.

The short-lived OH radical oxidizes many gases in the atmosphere. Globally averaged, most of the OH reacts with either CO or methane. In our scheme the explicit oxidation of methane and other hydrocarbons is left out. Instead, a generic hydrocarbon RH is introduced, which reacts identical to CO but with a different reaction rate which is controlled by the parameter f (see Table 1). The atmospheric lifetime of hydrocarbons ranges from many years (e.g., methane) to minutes, but almost all hydrocarbons are oxidized by OH, which stresses its important role in atmospheric chemistry. When OH reacts with CO, HO_2 is formed. We assume that the reaction between RH and OH produces only HO_2.

A constant mixing ratio of CO is used to represent all the hydrocarbons that live long compared to the turbulent timescale (e.g., methane and CO). RH is used to study the behavior of hydrocarbons which react with a timescale similar to the turbulent timescale.

2.2. Model Description

The CBL is simulated by means of a LES model. A detailed description of the model is given by *Molemaker and Vilà-Guerau de Arellano* [1998]. Briefly, the CBL is generated by a prescribed heat flux at the surface (0.1 K m s^{-1}). A convective layer is developed with a height H of 1000 m and a convective velocity scale w^* of 1.5 m s^{-1}. These length and velocity scales define an integral turbulent timescale (H/w^*) of approximately 11 min. This timescale will be used to characterize the influence of convective turbulence on the chemical transformations.

The difference between the LES model that is used in the present work (and by *Molemaker and Vilà-Guerau de Arellano* [1998]) and most other LES models [*Mo-*

eng and Wyngaard, 1984, 1989; *Schumann*, 1989] is the subgrid scale model. It has been shown by *Nieuwstadt et al.* [1993] and *Beets et al.* [1996] that, for convective conditions, different subgrid models do not lead to significant differences in the results. This is the motivation for using the most simple subgrid model possible, namely, a constant subgrid diffusivity with a value of 7 m^2 s^{-1}.

It can be inferred from *Molemaker and Vilà-Guerau de Arellano* [1998] that the smallest (dimensionless) length scale of the flow that contains energy can be calculated from

$$\eta = (1/Ra_f)^{1/4}, \tag{2}$$

with Ra_f the flux Rayleigh number (10^7). The corresponding dimensional value amounts to about 18 m. Combined with the subgrid scale diffusivity of 7 m^2 s^{-1}, the smallest resolved timescale of the flow is about 45 s.

The spatial domain that has been simulated is $4 \times 4 \times 1$ km. In the horizontal domain, periodic boundary conditions are assumed. The upper boundary is considered to be a rigid lid ($w = 0$). It has been shown by *Molemaker and Vilà-Guerau de Arellano* [1998] that the segregation between reacting top-down and bottom-up scalars can be adequately simulated with such a rigid lid upper boundary condition. Their results compare well with results reported by *Schumann* [1989], who simulated an entraining boundary layer based on the work of *Moeng and Wyngaard* [1984, 1989].

To account for the exchange of species with the overlying free troposphere, an exchange flux is calculated according to

$$\phi_e = w_e\ (c_{CBL} - c_{FT}), \tag{3}$$

Table 2. Subgrid Scale Damköhler Numbers (Equation (6)) for the Chemical Reactions of the Species Described in Table 1

	O_3	NO	NO_2	RH	HO_2	OH
Concentration, ppb	68.8	0.138	0.608	3.00	35.1*	0.537*
Emission flux, ppb m s^{-1}	—	0.1	—	1.0	—	—
v_d, cm s^{-1}	0.5	0.2	0.5	0.1	1.0	1.0
J_1	-1.2×10^{-4}	—	—	—	—	+30
J_2	$+3.5\times10^{-3}$	+1.8	-0.40	—	—	—
k_1	-2.9×10^{-3}	-1.5	+0.33	—	—	—
k_2	—	—	—	—	+0.41	-27
$k_2 \times 100$	—	—	—	-1.4×10^{-2}	+1.2	-81
k_3	—	-0.33	$+7.5\times10^{-2}$	—	-1.3	+85
k_4	-7.9×10^{-5}	—	—	—	-0.15	+10
k_5	—	—	—	—	-0.23	—
k_6	—	—	-6.6×10^{-3}	—	—	-7.5
k_7	-4.2×10^{-5}	—	—	—	$+8.3\times10^{-2}$	-5.4
k_8	—	—	—	—	-6.6×10^{-2}	-4.3

A minus (plus) sign indicates that species are depleted (produced). The volume-averaged concentrations that have been used in the calculations are given on the first row. The second and third row contain the emissions and deposition velocities that are used in the simulation.

*Concentration in units ppt for HO_2 and OH.

where a ϕ_e is the flux (ppb m s^{-1}, positive means upward), w_e is the exchange velocity (m s^{-1}), and c_{CBL} and c_{FT} (ppb) are the concentrations in the CBL and free troposphere, respectively. The concentrations in the free troposphere are taken as O_3, 50 ppb; NO_x, 50 ppt (parts per trillion); CO, 100 ppb; RH, 0 ppb. The corresponding concentrations of NO, NO_2 OH, and HO_2 are calculated by integrating the chemical rate equations to steady state with the rates given in Table 1. The resulting concentrations in the free troposphere are NO,11.4 ppt; NO_2, 38.6 ppt; HO_2, 33.5 ppt; OH, 0.548 ppt.

At the bottom and the top of the model domain, stress-free boundary conditions are prescribed. *Molemaker and Vilà-Guerau de Arellano* [1998] showed that the results obtained with these boundary conditions compared well with other LES models [*Moeng and Wyngaard*, 1984, 1989] and laboratory experiments [*Deardorff*, 1966]. At the surface, RH and NO are emitted and all species are removed by deposition. A (dry) deposition flux is calculated as the product of a species-dependent deposition velocity and the surface concentration. Deposition velocities for O_3 and NO_2 are estimated from a study of *Ganzeveld and Lelieveld* [1995]. The choice of the other deposition velocities is rather arbitrary, since deposition is an unimportant process for the remaining species. Deposition velocities of the species are listed in Table 2.

Most of the results that are presented were obtained at a resolution of 128 × 128 × 64 grid cells. Results obtained at a coarser resolution are almost identical (volume-averaged concentrations differ less than 0.3%). Therefore all sensitivity runs were performed with a resolution of 64 × 64 × 32. The simulations that are presented correspond to the case $f=100$, CO fixed at 100 ppb, $w_e = 0.01$ m s^{-1}, and RH and NO emission fluxes of 1.0 and 0.1 ppb m s^{-1}, respectively. The RH flux is inspired on isoprene flux measurements given by *Jacob and Wofsy* [1988]. Maximum isoprene emission fluxes of 0.4 ppb m s^{-1} were measured in a tropical forest. Since our RH species represents all reactive hydrocarbons and intermediates, a value of 1 ppb m s^{-1} seems a realistic value, which can also be representative of NMHC emissions from combustion processes. The selected NO flux is typical for an agricultural area. Sensitivity runs will be presented for lower emission fluxes, different RH/NO emission flux ratios, and different values for w_e.

Apart from the thermodynamic equations, the conservation equations of the variable chemical species are solved. The potential temperature is initialized with an exponentially decaying profile with random fluctuations to speed up the initialization process. All initial velocities are set to zero and an integration is carried out for at least 2 hours. The first integration hour is not considered in order to allow the turbulence to develop and to allow the chemistry to reach a (pseudo) steady state. The discretized differential equations for heat, momentum, and chemical species are integrated in time using an Adams-Bashfort method as described by *Molemaker and Vilà-Guerau de Arellano* [1998]. Note that the differential equations of the chemical species are solved using the same method as the heat and mo-

mentum equations. A time step of about 1.5 s turned out to be sufficient to suppress the growth of small numerical instabilities that are due to the central differences scheme.

2.3. Simulation Strategy

The photochemistry scheme presented in Table 1 is studied. The chemical transformations in the convective flow are simulated until a (pseudo) stationary state is reached. Such a stationary situation is defined by (almost) constant values of the volume-averaged and horizontally averaged quantities in the model. Since the slowest chemistry timescale is rather long (see Table 2), a true stationary state is reached only after a long integration time (i.e., several days).

To start as close as possible to a chemical steady state, the chemistry scheme is first integrated to steady state in a box model which is operated with the same boundary conditions and rate constants. The resulting concentrations (see Table 2) are used as homogeneous initial concentration fields in the three-dimensional model. Basically, two mechanisms can lead to differences with the concentrations calculated in the box model:

1. In the box model the deposition term is calculated using the box model concentration. In the LES the concentration at the surface is used to calculate the deposition term. The 3-D concentration fields are influenced by turbulence, emission, and deposition. In general, the LES surface concentration is different from the box model concentration, which leads to differences in the deposition term.

2. The turbulent structure generates concentration fluctuations in the LES domain. Therefore the volume-averaged rate of the chemical transformations may differ from the box model. A proper dimensionless number to quantify the effect of concentration fluctuations on the volume-averaged reaction rate between two species A and B is the volume-integrated intensity of segregation ($< I_s >$), which is defined as [Brodkey, 1981]

$$< I_{s,A+B} > = \frac{< A'B' >}{< A >< B >}, \qquad (4)$$

where $A'B'$ represents the covariance between species A and B, angle brackets are the volume-averaging operator, and a prime stands for deviations from the average. In the box model and in the case of well-mixed species in the LES, the value of $< I_s >$ is zero. The intensity of segregation between two reacting species is a measure of the effect of incomplete mixing on chemical transformation because the volume-averaged reaction rate can be written as

$$< k_{A+B} > = k_{A+B}(1+ < I_{s,A+B} >). \qquad (5)$$

The intensity of segregation $< I_s >$ can also be interpreted as a measure of the deviations from chemical equilibrium due to atmospheric processes. Note that (5)

appears in the volume-averaged conservation equation.

Throughout the rest of this paper, angle brackets will denote a volume-averaged quantity and an overbar will denote a horizontally averaged quantity. For instance, $\overline{w'RH'}(z)$ denotes the horizontally averaged flux of RH at height z.

2.4. Modeling the Subgrid Scale Chemistry

The range of scales in the ABL encompasses many orders of magnitude, from the height of the layer which is $\mathcal{O}(10^3$ m), to the Kolmogorov scale that is $\mathcal{O}(10^{-3}$ m). Any present-day numerical model is only capable of simulating 2 orders of magnitude in scales. A LES model solves the most relevant (energetic) scales of the turbulence and parameterizes the contributions of the subgrid scales.

It is important to note that two reacting chemical compounds may have a significant covariance at spatial scales smaller than the grid size. When this subgrid scale (SGS) segregation is important, its effect on the chemistry must be taken into account. In order to determine if SGS segregation is important, Molemaker and Vilà-Guerau de Arellano [1998] introduced the subgrid scale Damköhler number (Da_k) for a binary reaction. This dimensionless number is defined as

$$Da_k = \frac{\tau_s}{\tau_{chem}}, \qquad (6)$$

where τ_s is the smallest resolved flow timescale (45 s, see section 2.2) and τ_{chem} is the timescale of chemistry. $|Da_k| > 1$ implies that one has to account for segregation of the reacting species at SGS. For $|Da_k| < 1$ all the relevant scales of the reacting species are adequately solved by means of the LES.

For a more complex chemical scheme the definition of a timescale for each reacting compound is not so straightforward. The rate of change of chemical active species is controlled by many reactions and each reaction is characterized by its own timescale.

For the chemistry studied here, Table 2 lists the Da_k values for all species and all reactions. These values have been calculated with a timescale of the smallest resolved eddies of 45 s and the concentrations listed on the top row of the table. These concentrations refer to steady state box model values which are calculated given the emission fluxes and deposition velocities on the second and third row of the table. The exchange velocity with the overlying atmospheric layer was taken as 0.01 m s^{-1}. The species' concentrations in this layer were listed in section 2.2. Note that negative values in Table 2 refer to chemical depletion. As an example, the value of Da_k for OH formation by reaction J_1 is calculated as $\tau_s (2J_1O_3/OH)$.

In Table 2 it is shown that the OH rate equation is governed by very fast chemical reactions ($|Da_k| >> 1$). The associated OH timescale is therefore very small compared to the smallest resolved flow timescale. How-
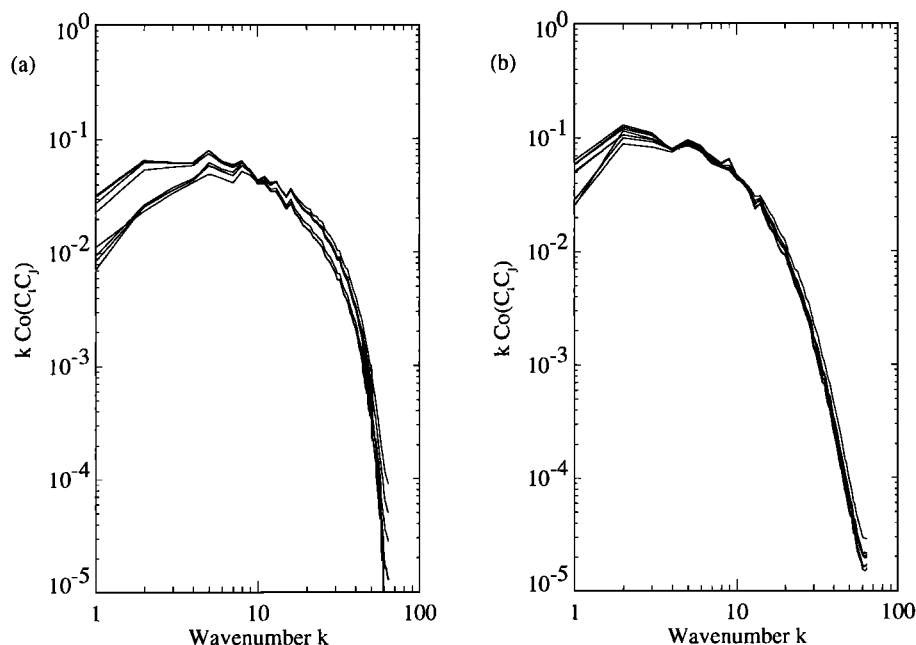
Figure 1. Cospectra of the reacting concentration fields (multiplied by the wavenumber k and normalized to an integrated value of 1) at (a) $z/H = 0.008$ and (b) $z/H = 0.5$ obtained at a resolution of $128 \times 128 \times 64$ grid cells. The spectra have been obtained by averaging the 128 horizontal line spectra at the specified heights. Additionally, the spectra have been time averaged over the last 20 min of a 3 hour run.

ever, as we show below, $|Da_k| > 1$ does not necessarily lead to a significant segregation at the SGS.

For a binary reaction between A and B, *Schumann* [1989] calculated the cospectra [*Stull*, 1988] of the reacting concentration fields. By analyzing the contributions of the different spatial scales to the covariance, he could determine that the SGS segregation was negligible. A cospectrum that falls off sharply at the higher wavenumbers indicates that the unresolved scales do not contribute significantly to the total covariance, since the value of the cospectrum at the highest wavenumbers is a measure for the covariance at the smallest scales.

Following this approach, Figure 1 shows the cospectra for all the reacting concentration fields. The eight bimolecular reactions between the variable species listed in Table 1 result in eight cospectra. Figures 1a and 1b show the cospectra at $z/H = 0.008$ and $z/H = 0.5$, respectively. By comparing Figures 1a and 1b it is clear that the covariance at the smaller scales is more important near the surface than in the bulk, because less energy is at the smaller scales in Figure 1b. However, for the resolution used for the simulation ($128 \times 128 \times 64$) the cospectra fall off rapidly both in the bulk and near the surface. This means that not much energy is left for the SGS. In conclusion, the SGS covariances can be neglected and no parameterization of these terms is required.

3. Results

Figure 2 shows the typical time evolution of the concentrations in the model layer adjacent to the surface ($z/H = 0.008$) and halfway the model domain ($z/H = 0.5$). Although the emissions are uniformly distributed across the surface, the flow field induces large concentration fluctuations. These fluctuations are more pronounced close to the surface, although, for instance, RH shows considerable concentration variations at $z/H = 0.5$.

Concentration fluctuations are rather small for ozone. NO, RH and NO_2 are strongly correlated since these species are emitted at, or produced close to, the surface. OH is shown for completeness, since its concentration is fully determined by the other species (see section 2.4). Table 3 lists the volume-averaged intensities of segregation between all the species, the steady state box model concentrations, and the volume-averaged concentrations after 3 hours of simulation. The values are all close to steady state and have been averaged over the last 20 min of the simulation. Positive values for $< I_s >$ are found between RH, NO, and NO_2. The instantaneous concentrations (Figure 2) show the same correlations. This illustrates the general overturning circulation of the CBL: updrafts carry the emitted species upwards and the downdrafts contain less RH and NO_x ($NO + NO_2$) due to depletion by chemical reactions.
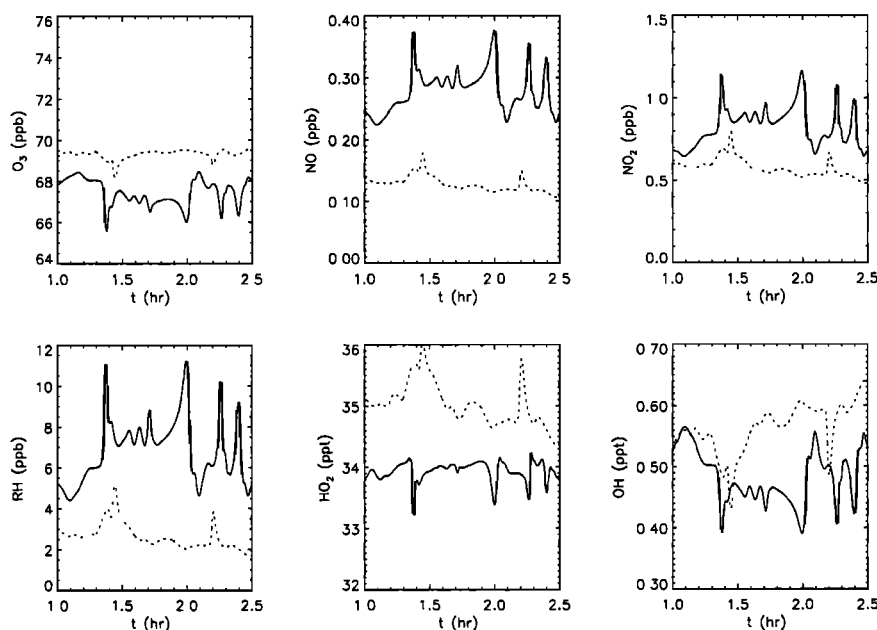
Figure 2. Time series of the instantaneous concentrations at $z/H = 0.5$ (dotted line) and $z/H = 0.008$ (solid line). Concentrations are shown in the center of the horizontal domain.

The averaged LES concentrations do not differ substantially from the box model concentrations. Minor differences are caused by the small intensities of segregation between the reacting species (numbers in parentheses in Table 3) or differences in deposition (see section 2.3). Only the reactions between RH and OH, and between NO_2 and OH are decelerated due to segregation effects by 3.4% and 1.3%, respectively.

Figure 3 shows the horizontally averaged vertical concentration profiles. The bars represent the standard deviations from the horizontal averages and show that the concentration fluctuations are more pronounced close to the surface. All profiles indicate that larger gradients exist close to the surface due to emissions and dry deposition.

The vertical flux profiles are shown in Figure 4. Note that the vertical flux consists of a resolved contribution and a SGS contribution. The latter part is modeled by a diffusion process. It can be seen that for species such as NO and HO_2 the vertical profiles deviate significantly from a linear profile.

The strongest effects of chemistry are manifest in the NO and NO_2 fluxes. At the surface, the NO_2 flux is negative due to deposition. Close to the surface, chemical production of NO_2 changes the sign of the flux. NO_2 is mainly produced by the reaction between NO and O_3. Therefore the NO flux profile is also influenced by chemistry. However, the NO_x (NO + NO_2) profile is almost linear, because the overall chemical depletion of nitrogen species is a slow process relative to the mixing in the CBL.

4. Discussion

4.1. Segregation in the CBL

Previous LES results in the CBL [*Schumann*, 1989; *Sykes et al.*, 1994; *Molemaker and Vilà-Guerau de Arellano*, 1998] revealed that the effects of incomplete mixing on the chemical transformations are potentially very important. These results were obtained for a reaction between two species which are emitted at the surface (species A) and entrained from aloft (species B).

If the chemical timescale of the reaction between A and B becomes comparable to or smaller than the mixing timescale, the largest segregation effects are observed. The ratio of these two timescales is defined as the turbulent Damköhler number:

$$Da_t = \frac{\tau_t}{\tau_{chem}} \qquad (7)$$

where τ_t stands for the turbulent timescale (here about 11 min, see section 2.2), and τ_{chem} for a chemistry timescale. A value of Da_t which is close to 1 indicates possible effects of the turbulent mixing on the chemical transformation. The intensity of segregation can thus be minimized (the minimum value is -1) by imposing equal fluxes of A and B with opposite sign and by imposing a chemical lifetime that is close to the turbulent timescale. *Schumann* [1989] showed that the $< I_s >$ between species A and B diminishes when the ratio of the emission fluxes deviates from unity. In that case, either A or B will be in excess which suppresses the intensity of segregation.
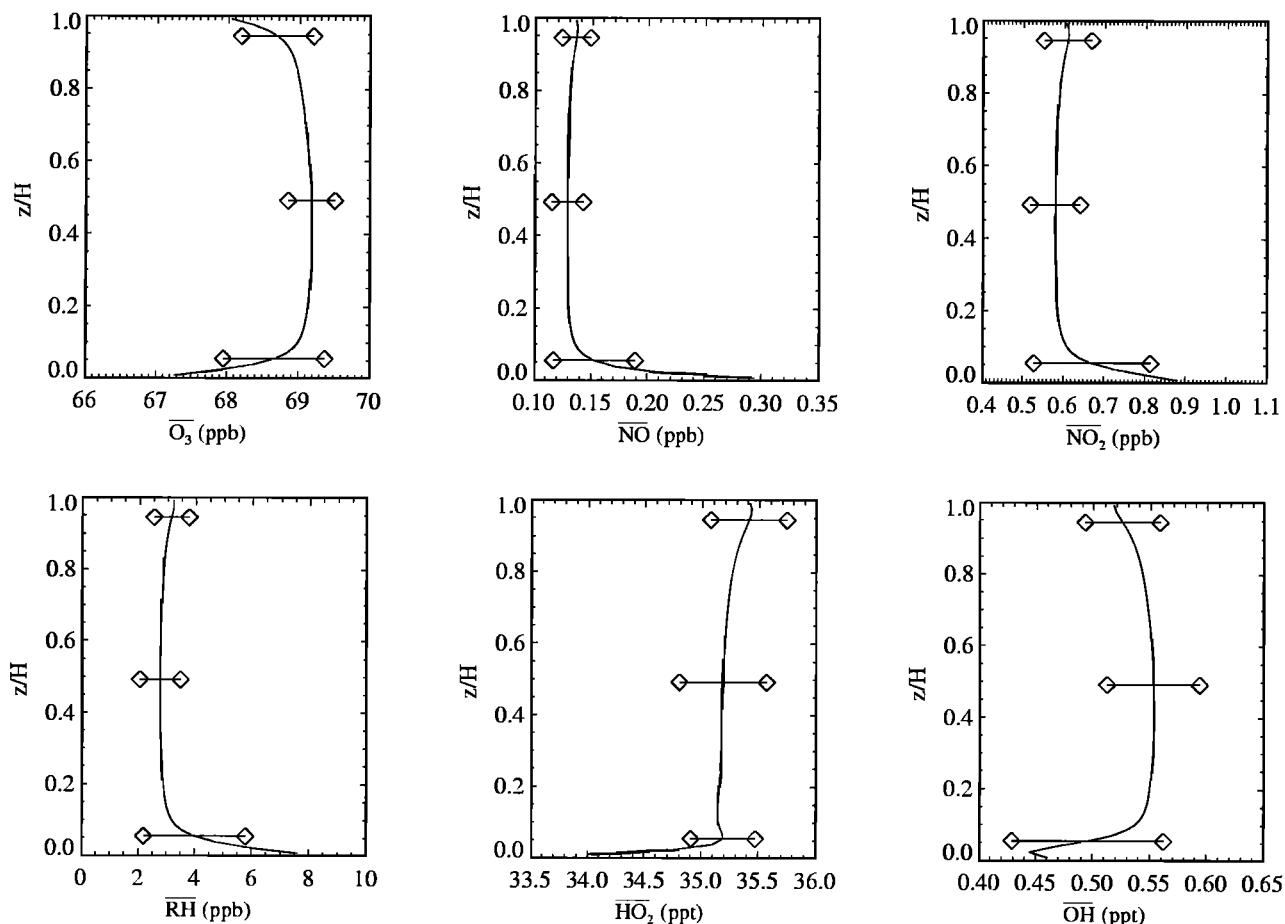
Figure 3. Vertical profiles of the concentrations. The vertical axis shows the nondimensional height. The bars denote the standard deviation of the horizontal average at $z/H = 0.05, 0.5$, and 0.95. The profiles have been averaged over the last 20 min of the simulation.

The extension of the previous studies to a more complex chemistry scheme leads to substantially different findings. In the chemical scheme that is studied here, one or more of the conditions that produces segregation between the species is violated. For instance, the NO and O_3 fluxes are not opposite in sign. Moreover, NO and O_3 are chemically produced by means of NO_2 photolysis.

In order to explain the low values of $< I_s >$ for chemical reactions with $|Da_t| \geq 1$, we analyze the chemical terms in the NO rate equation, which reads

$$\frac{\partial NO}{\partial t}\bigg|_{chem} = J_2 NO_2 - NO\ (k_1 O_3 + k_3 HO_2\ ). \quad (8)$$

The net chemical tendency of NO is determined by the sum of a large production and a large destruction term. The overall timescale that is associated with this chemical tendency is usually much smaller than the timescales of the individual reactions. This is illustrated in Figure 5 which shows the horizontally averaged Da_t values for NO. At $z/H > 0.1$ the sum of the large individual terms approaches zero. This means that in the bulk of the CBL, NO is in photostationary state:

$$J_2 \frac{NO_2}{NO} \approx k_1 O_3 + k_3 HO_2. \quad (9)$$

This near balance between chemical production and destruction of NO is perturbed by physical processes like deposition, emission, and advection. Especially NO emissions at the surface considerably perturb the chemical balance.

The chemical species that participate in chemical cycles like the photostationary state (equation (9)) are continuously produced and consumed at a rate that exceeds the mixing rate in the CBL. This can be directly inferred from the Da_t values that are presented in Figure 5. This results in well-mixed distributions (e.g., O_3) and low values of the $< I_s >$ (e.g., for the NO + O_3 reaction). Even for the self-reaction of HO_2 (concentration variations of HO_2 lead, by definition, to a positive $< I_s >$) only a minor effect is found.

RH is the only variable species that does not participate in fast production and loss processes. Due to its high reactivity (for $f = 100$), RH is an important sink for OH. This means that OH will be suppressed in regions of high RH concentrations, which explains the negative $< I_s >$ for the reaction between RH and OH.
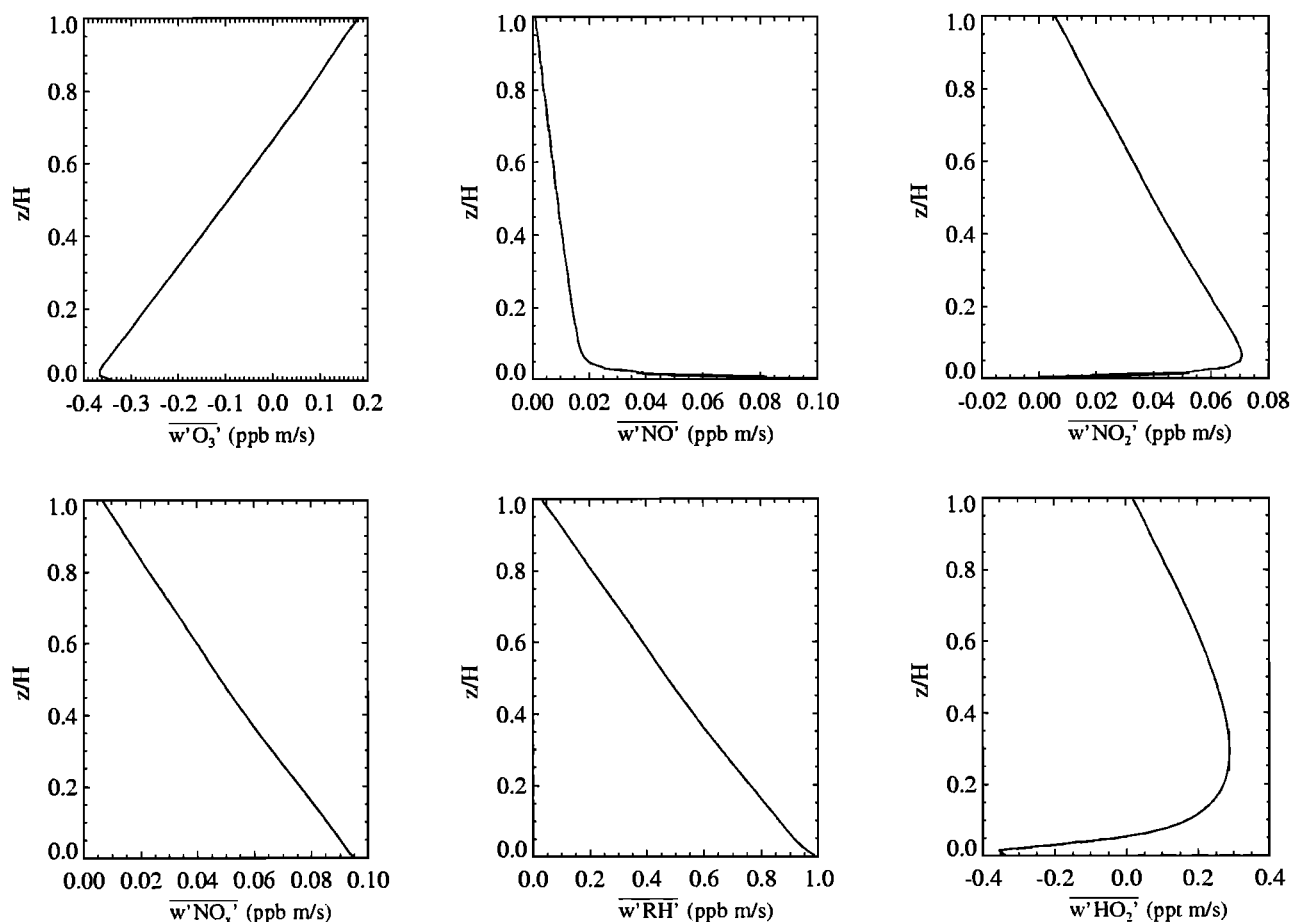
Figure 4. Vertical flux profiles of all the species except OH. As indicated in the text, the sum of the NO and NO_2 fluxes (the NO_x flux) is also shown. The profiles result from averaging over the last 20 min of the simulation.

In the next section it will be shown that these effects are more pronounced when RH is nonuniformly emitted.

4.2. Segregation Between RH and OH

Global or regional atmospheric chemistry simulations can not resolve highly localized emissions. Potentially, the effect of these local emissions is large because the chemistry is highly nonlinear. Therefore a large local emission has a different effect on chemical transformations than uniform emissions with the same total source strength [*Mathur et al.*, 1992; *Chock et al.*, 1996; *Sillman et al.*, 1990; *Vilà-Guerau de Arellano et al.*, 1993].

LES offers the opportunity to study this effect for a realistic turbulent flow. For this purpose, RH and NO are emitted at the surface by means of a Gaussian emission function that leaves the total emitted amount unchanged. The emissions are distributed according to

$$d(x,y) = \exp\left(-30\left[(x-0.5)^2 + (y-0.5)^2\right]\right), \quad (10)$$

where x and y run from 0 to 1 in the horizontal domain. The result of this emission distribution is that the emission in the center $((x,y) = (0.5, 0.5))$ is about 10 times larger than the average emission strength. A Gaussian

emission distribution is selected because its smoothness introduces less numerical instabilities than a more realistic distribution would do. The purpose here is to show the possible effect of non-homogeneous emissions on the intensity of segregation.

Figure 6 shows the time evolution of the calculated $< I_s >$ for the RH–OH and NO_2–OH reactions together with the results for the case with uniform emissions. In both runs the rate coefficient for the RH–OH reaction is taken as $k_2 \times 100$. For this rate and an OH concentration of 0.5 ppt, the chemical lifetime of RH amounts to about 0.8 hour.

After pseudo-steady state is reached, the RH–OH segregation reaches values between 15 and 20%. In other words, the volume-averaged reaction is retarded by 15–20% compared to the box model. This effect is caused by the large RH concentration fluctuations in the case of a nonuniform emission distribution. For instance, close to the emission center concentrations exceeding 50 ppb are encountered, whereas in regions near the domain margin negligible concentrations are found.

Although turbulent mixing tends to annihilate these concentration differences, the chemical breakdown of

Table 3. Volume-Averaged LES Concentrations, Box Model Concentrations, and Intensities of Segregation Between the Chemical Species

	O_3	NO	NO_2	RH	HO_2	OH
LES, ppb	69.0	0.136	0.601	3.05	35.2*	0.541*
box, ppb	68.8	0.138	0.608	3.00	35.1*	0.537*
O_3	+0.01	—	—	—	—	—
NO	(-0.13)	+4.8	—	—	—	—
NO_2	-0.09	+3.2	+2.4	—	—	—
RH	-0.24	+8.5	+6.2	+16.0	—	—
HO_2	(-0.00)	(+0.02)	+0.07	+0.12	(+0.01)	—
OH	(+0.05)	-1.7	(-1.3)	(-3.4)	(-0.07)	+0.9

The intensities of segregation are expressed in percent and are calculated as $100 \times <A'B'> / <A><B>$. Numbers in parentheses refer to pairs of reacting species. The values have been averaged over the last 20 min of a 3 hour run.
*Concentration in units ppt for HO_2 and OH.

RH is fast enough to preserve the strong concentration gradients. The segregation between NO_2 and OH is caused by the fact that the RH and NO (which is quickly converted to NO_2) are co-emitted.

The segregation between RH and OH has direct consequences for their volume-averaged concentrations. Initially, both < OH > and < RH > increase compared to the steady state box model values because they are both consumed at a slower rate (see equation (5)).

Figure 7 shows that the initial < OH > increases are counteracted by the increasing < RH > and that

< OH > in pseudo-steady state is only slightly higher than the box model concentration. The < RH > concentration becomes larger than the box model by an amount (in percent) that is approximately equal to < I_s >. The effect on other species is less significant.

One topic that has not been discussed so far is the vertical variation of I_s. For that purpose, Figure 8 shows the vertical intensity of segregation profile for the RH–OH reaction:

$$\overline{I_{s,\text{RH+OH}}}(z) = \frac{\overline{RH'OH'}(z)}{\overline{RH}(z)\overline{OH}(z)}. \tag{11}$$

The results are shown for the case of nonuniform and uniform emissions. In the case of uniform emissions the segregation is purely caused by the RH concentration differences (and the anticorrelated differences in OH) between the updrafts and downdrafts. The highest segregation effect are found at heights just above the surface. In the case of nonuniform emissions, the emission field itself generates horizontal variations in RH. As a result, the RH–OH segregation is much larger and has its maximum at the surface. In both cases, however, the general overturning circulation of the CBL can be discerned from the profiles. The higher values of $\overline{I_{s,\text{RH+OH}}}$ at the surface are transported upward by the thermal updrafts. These vertical motions are fast compared to horizontal mixing, which tends to destroy the horizontal segregation.

4.3. Sensitivity Analysis

The results that have been obtained so far can be summarized as follows: the segregation between reacting species in the CBL is generally very low (< 5%). The largest effects are found for the reaction between OH and a generic short-lived hydrocarbon RH. Other species are continuously produced and consumed at a rate that exceeds the mixing rate in the CBL. When RH is nonhomogeneously emitted, larger values for < I_s > are found due to larger RH concentration fluctuations.
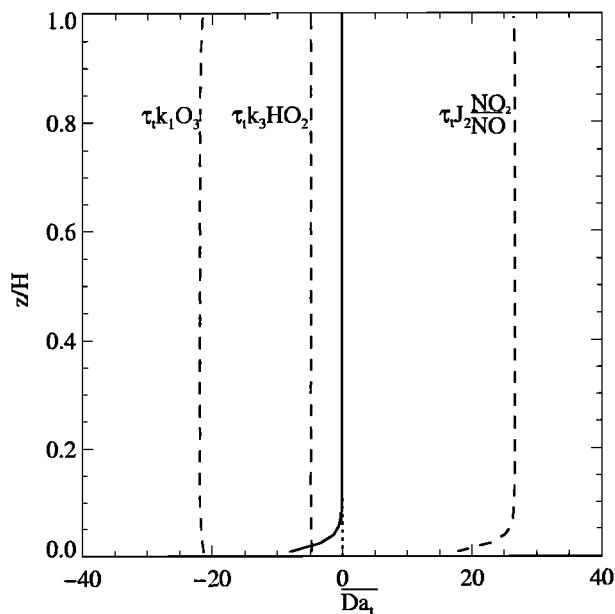

Figure 5. Vertical profiles of the horizontally averaged turbulent Damköhler numbers (equation (7)) for NO. The solid line (the overall Da_t) represents the sum of the dashed lines. The three dashed lines correspond to the three reactions in the NO chemical rate equation and are labeled by the corresponding expression for Da_t. The vertical axis shows the nondimensional height.
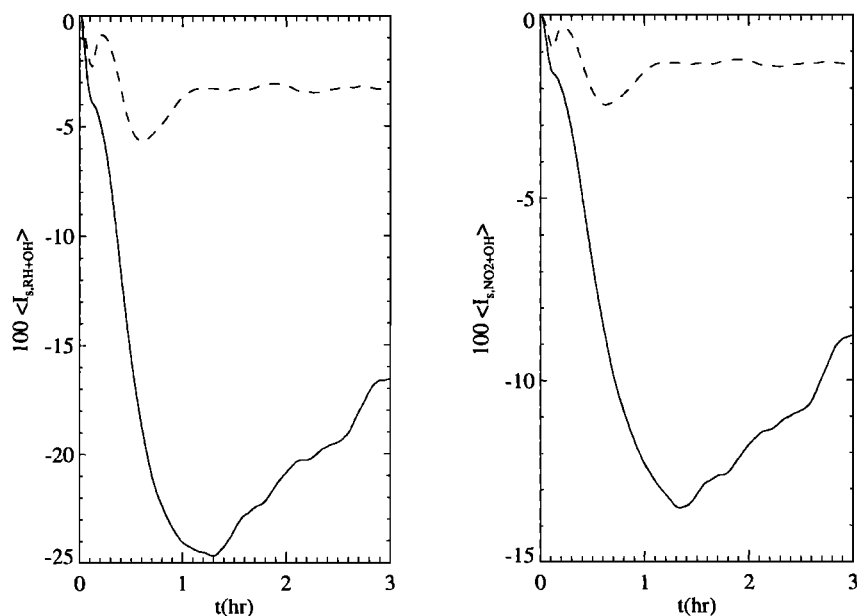
Figure 6. Time evolution of the intensity of segregation ($\times$ 100) between (left) RH and OH and (right) NO_2 and OH. Solid line, nonuniform emissions; dashed line, uniform emissions.

In this section we investigate the sensitivity of these results for various model parameters. More specifically, the following questions are addressed.

1. What is the effect of the entrainment velocity w_e?

2. What is the effect if only RH (or only NO) is emitted nonuniformly?

3. How sensitive are the results for the emission fluxes of RH and NO?

4. What is the sensitivity for the RH–OH reaction rate (parameter f)?

Table 4 contains the results for the sensitivity calculations that were performed. In each sensitivity simulation only one parameter was modified and the concentrations in the free troposphere remained unchanged. All simulations lasted at least 2 hours until quasi-steady state was reached. The different cases were initialized with the steady state box model concentrations that were obtained with the appropriate parameter values. The listed values for the segregation between RH and OH and between NO_2 and OH were averaged over the
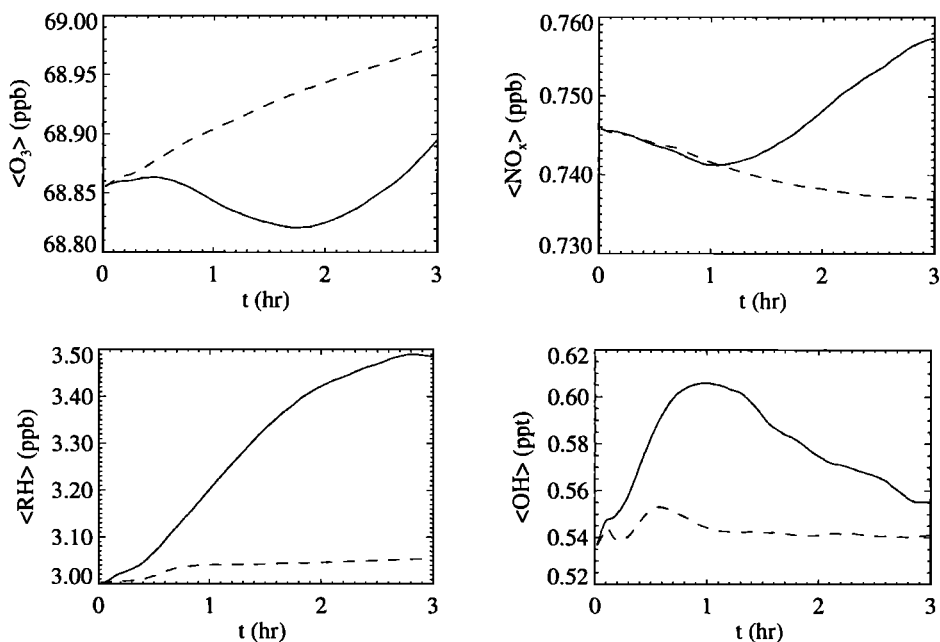

Figure 7. Time evolution of the volume-averaged concentrations of O_3, NO_x, RH, and OH. Solid line, nonuniform emissions; dashed line, uniform emissions.
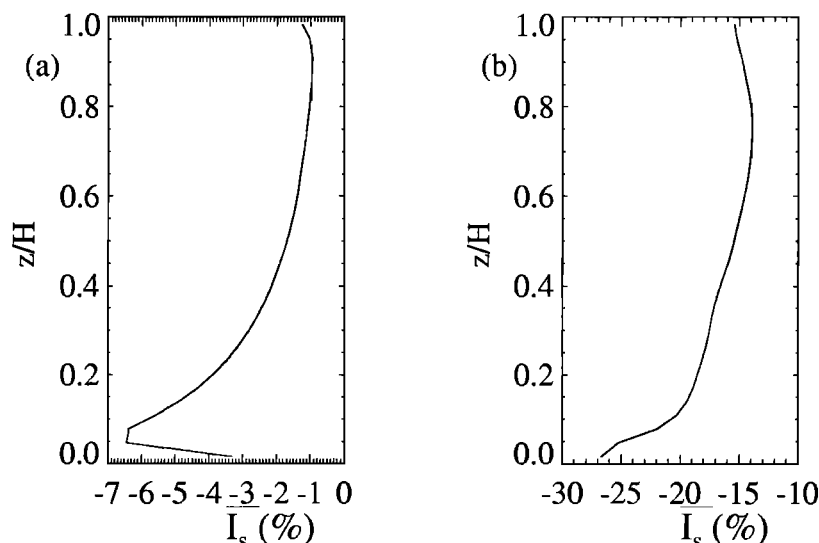
Figure 8. Horizontally averaged intensity of segregation ($\times 100$) between RH and OH (see equation (11)): (a) uniform emissions and (b) nonuniform emissions.

last 20 min of the simulation. Other $< I_s >$ values were small ($< 1\%$) and are not included in the table. Only for nonuniform emissions some values exceeded 1%, as will be noted below. From the sensitivity runs it can be concluded that the segregation effects do not depend strongly on the entrainment velocity w_e and the specific input fluxes F_{NO} and F_{RH}. In all simulations, the maximum values for $< I_s >$ are less than 5%. As could be expected, the segregation effects become smaller for smaller input fluxes.

If only RH is emitted nonhomogeneously, the RH–OH segregation increases sharply compared to the case in which NO is also emitted nonhomogeneously. When both NO and RH are nonuniformly emitted, NO fluctuations cause horizontal OH gradients (by means of the $HO_2 + NO$ reaction) that counteract the RH–OH segregation. The $HO_2 + NO$ reaction causes also a positive value of $< I_{s,NO_2+OH} >$ which is found when only NO is emitted nonuniformly. In that case, the strong localized NO emission causes a rather strong anticorrelation between NO and HO_2 ($I_{s,NO+HO_2} = -9.9\%$, not shown in the table). The reaction products of this reaction (NO_2 and OH) are positively correlated. Positive spatial correlation is also observed between NO and NO_2 ($< I_{s,NO-NO_2} > = 36\%$) and between NO and OH ($< I_{s,NO-OH} > = 6.3\%$).

Finally, the RH-OH segregation depends strongly on the reaction rate between these two species. If this rate is increased (by means of parameter f), the RH concentration variations become more and more pronounced. The updrafts transport RH-rich and OH-poor air. The downdrafts are on the average depleted in RH and enriched in OH. This effect becomes larger if the chemical lifetime of RH approaches the turbulent timescale τ_t. For $f = 300$ the chemical lifetime of RH in the

box model (0.54 ppt OH) is about 17 min compared to a turbulent timescale τ_t of 11 min. Due to segregation between OH and RH, the chemical lifetime of RH in the LES model is about 20% longer (see Table 4). It is important to note once more that these latter segregation effects are purely caused by the influence of the turbulence on the chemical reactions and not by nonuniform emissions.

Similar segregation effects have been addressed by *Davis* [1992], who studied the isoprene–OH reaction in the CBL. On the basis of 1-D model calculations he predicted only a small decrease in the reaction rate due to the negative covariance between OH and isoprene. These results are in good agreement with our results, since the lifetime of isoprene is a few hours in the CBL. However, a 1-D model can not simulate the larger gradients that are expected when the isoprene emissions are strongly localized.

Isoprene emissions in the boundary layer are not continuous. It has been observed that the emissions are injected in the BL through intermittent gusts [*Gao and Li*, 1993; *Turner et al.*, 1994]. The LES calculations with a spatially nonuniform emission distribution indicate that such an intermittent emission pattern might have a retarding effect on the isoprene oxidation rate. It is also shown here that these effects become more important if the species are readily oxidized by OH. Recent OH measurements reported by *Mount et al.* [1997] show that the in situ measured surface OH concentrations are lower than OH concentrations measured by a long-path absorption technique. The in situ measurements have been analyzed with a box model by *McKeen et al.* [1997] (see also *Comes et al.* [1997]). But it is shown in the present study that such a box model approach may underestimate OH if localized reactive hydrocarbon emissions occur. Because of their high reactivity

Table 4. Intensity of Segregation Between RH and OH and Between NO_2 and OH for a Number of Sensitivity Runs

Q	w_e	F_{NO}	F_{RH}	f	$< I_{s,RH+OH} >$	$< I_{s,NO_2+OH} >$
ref (U)	0.01	0.10 (U)	1.0 (U)	100	-3.4	-1.3
ref (N)	0.01	0.10 (N)	1.0 (N)	100	-17.8	-9.6
1	0.00	0.10 (U)	1.0 (U)	100	-3.4	-1.3
1	0.03	0.10 (U)	1.0 (U)	100	-3.2	-1.4
2	0.01	0.10 (U)	1.0 (N)	100	-29.4	-2.1
2	0.01	0.10 (N)	1.0 (U)	100	-5.4	+5.7
3	0.01	0.10 (U)	0.5 (U)	100	-2.8	-1.1
3	0.01	0.10 (U)	0.2 (U)	100	-0.8	-0.3
3	0.01	0.05 (U)	0.5 (U)	100	-2.4	-0.9
3	0.01	0.05 (U)	0.2 (U)	100	-0.7	-0.3
3	0.01	0.01 (U)	0.1 (U)	100	-0.5	-0.2
4	0.01	0.10 (U)	1.0 (U)	200	-11.5	-2.7
4	0.01	0.10 (U)	1.0 (U)	300	-20.5	-3.8

Intensity of segregation is $100 \times < I_s >$ in percent. Parameters that have been varied are the entrainment velocity w_e (m s^{-1}), the RH flux F_{RH}, the NO flux F_{NO} (both in ppb m s^{-1}), and f (see Table 1). U refers to uniform emissions; N refers to nonuniform emissions of RH and/or NO (equation (10)). The first two rows refer to the calculations with uniform and nonuniform emissions discussed in the previous sections. Q refers to the numbered questions in the text.

these compounds are difficult to detect experimentally, which introduces additional uncertainties.

Another important conclusion is that the neglect of the effects of turbulence on chemical transformations in large-scale global or regional models does not introduce large errors. Only highly reactive hydrocarbons and strong localized emissions of, for example, NO deserve extra attention. However, we have not studied the effects of the diurnal variations in the photolysis rates and in the boundary layer structure. These effects might considerably perturb the chemical equilibrium to which this study was restricted.

5. Summary and Conclusions

Daytime photochemistry is studied in the convective atmospheric boundary layer by means of a three-dimensional large-eddy simulation model. The main conclusions can be summarized as follows.

1. The turbulent flow field induces large concentration fluctuations. These variations are strongest near the surface, but they can persist in the bulk of the CBL. These concentration fluctuations imply that the concentrations deviate from the chemical equilibrium that is obtained in a box model calculation.

2. If the species are emitted uniformly, the volume-averaged concentrations deviate only slightly from box model concentrations. The largest effect is found for the relatively fast RH-OH reaction, which is slowed down by approximately 3% compared to the box model simulation. We analyzed the causes for these small effects. Species are involved in chemical cycles with chemical production and loss processes almost in balance. As a

result, the overall timescale that is associated with the chemical tendencies is usually much smaller than the timescale of the individual production and loss reactions. The fact that the overall timescale is smaller than the turbulent timescale explains the relatively small segregation of the compounds.

3. When RH is emitted nonuniformly (e.g., a varying source strength at the surface), larger segregation effects are found. In such cases, the intensity of segregation between RH and OH can reach values between 15 and 30%, depending on the nature of the NO emissions. Because RH is a major sink for OH, the high spatial variability of RH generates a high and anticorrelated variability in OH.

4. The spatial variability of RH is also enhanced when the reaction rate between RH and OH is increased (i.e., the turbulent Damköhler number of RH is increased). In other words, if the timescale of a compound is comparable to the turbulent timescale, the reaction rate with OH will slow down due to the chemistry-turbulence interaction.

These conclusions are obtained with a reduced chemistry scheme that is never far from steady state. This simplification enabled the study of segregation of reacting species in the CBL. Effects from varying photolysis rates, changing emissions, and nonsteady boundary layer heights have explicitly not been studied. Further research should focus on these factors.

References

Beets, C., M. Molemaker, and J. Vilà-Guerau de Arellano, Direct numerical simualtion and large-eddy simulation of a non-premixed binary reaction in a turbulent convective boundary layer, in *Engineering Turbulence Modelling and Experiments*, vol. 3, pp. 279–287, Elsevier Science, Netherlands, 1996.

Brodkey, R. S., Fundamentals of turbulent motion, mixing and kinetics, *Chem. Eng. Commun.*, 8, 1–23, 1981.

Chock, D. P., P. Sun, and S. L. Winkler, Trajectory grid: An accurate sign-preserving advection-diffusion approach for air quality modelling, *Atmos. Environ.*, 30, 857–868, 1996.

Comes, F. J., O. Forberich, and J. Walter, OH field measurements: A critical input into model calculations on atmospheric chemistry, *J. Atmos. Sci.*, 54, 1886–1894, 1997.

Davis, K. J., Surface fluxes of trace gases derived from convective-layer profiles, NCAR Coop.Thesis 139, Natl. Cent. for Atmos. Res., Boulder, Colo., 1992.

Deardorff, J., The counter-gradient heat flux in the lower atmosphere and in the laboratory, *J. Atmos. Sci.*, 23, 1538–1558, 1966.

Ganzeveld, L., and J. Lelieveld, Dry deposition parameterization in a chemistry general circulation model and its influence on the distribution of reactive trace gases, *J. Geophys. Res.*, 100, 20,999–21,012, 1995.

Gao, W., and B. L. Li, Wavelet analysis of coherent structures in the atmosphere-forest interface, *J. Appl. Meteorol.*, 32, 1717–1735, 1993.

Gao, W., and M. L. Wesely, Numerical modeling of the turbulent fluxes of chemically reactive trace gases in the atmospheric boundary layer, *J. Appl. Meteorol.*, 33, 835–847, 1994.

Jacob, D., and S. Wofsy, Photochemistry of biogenic emissions over the Amazon forest, *J. Geophys. Res.*, 93, 1477–1486, 1988.

Kley, D., Tropospheric chemistry and transport, *Science*, 276, 1043–1045, 1997.

Krol, M. C., and D. Poppe, Nonlinear dynamics in atmospheric chemistry rate equations, *J. Atmos. Chem.*, 29, 1–16, 1998.

Mathur, R., L. K. Peters, and R. D. Saylor, Sub-grid representation of emission source clusters in regional air quality modeling, *Atmos. Environ.*, 26, 3219–3238, 1992.

McKeen, S. A., et al., Photochemical modeling of hydroxyl and its relationship to other species during the Tropospheric OH Photochemistry Experiment, *J. Geophys. Res.*, 102, 6467–6493, 1997.

Moeng, C., and J. Wyngaard, Statistics of conservative scalars in the convective boundary layer, *J. Atmos. Sci.*, 41, 3161–3169, 1984.

Moeng, C., and J. Wyngaard, Evaluation of turbulent transport and dissipation closures in second-order modelling, *J. Atmos. Sci.*, 46, 2311–2330, 1989.

Molemaker, M. J., and J. Vilà-Guerau de Arellano, Turbulent control of chemical reactions in the convective boundary layer, *J. Atmos. Sci.*, 55, 568–579, 1998.

Mount, G. H., F. L. Eisele, D. J. Tanner, J. W. Brault, P. V. Johnston, J. W. Harder, E. J. Williams, A. Fried, and R. Shetter, An intercomparison of spectroscopic laser long-path and ion-assisted in situ measurements of hydroxyl concentrations during the Tropospheric OH Photochemistry Experiment, fall 1993, *J. Geophys. Res.*, 102, 6437–6455, 1997.

Nieuwstadt, F., P. Mason, C. Moeng, and U. Schumann, Large-eddy simulation of the convective boundary layer: A comparison of four computer codes, in *Turbulent Shear Flows*, vol. 8, pp. 343–367, Spinger Verlag, Berlin, 1993.

Peters, L., et al., The current state and future direction of eulerian models in simulating the tropospheric chemistry and transport of trace species: A review, *Atmos. Environ.*, 29, 189–222, 1995.

Petersen, A. C., C. Beets, H. van Dop, P. G. Duynkerke, and A. P. Siebesma, Mass-flux characteristics of reactive scalars in the convective boundary layer, *J. Atmos. Sci.*, 56, 37–56, 1999.

Poppe, D., and H. Lustfeld, Nonlinearities in the gas phase chemistry of the troposphere: Oscillating concentrations in a simplified mechanism, *J. Geophys. Res.*, 101, 14,373–14,380, 1996.

Schumann, U., Large-eddy simulation of turbulent diffusion with chemical reactions in the convective boundary layer, *Atmos. Environ.*, 23, 1713–1729, 1989.

Sillman, S., J. A. Logan, and S. C. Wofsky, A regional-scale model for photochemical production of ozone in the United States with subgrid representation of urban power plants, *J. Geophys. Res.*, 95, 5731–5748, 1990.

Stockwell, R. W., P. Middleton, J. S. Chang, and X. Tang, The second generation regional acid deposition model chemical mechanism for regional air qaulity modeling, *J. Geophys. Res.*, 95, 16,343–16,367, 1990.

Stull, R., *An Introduction to Boundary Layer Meteorology*. Kluwer Acad., Norwell, Mass., 1988.

Sykes, R. I., S. F. Parker, D. S. Henn, and W. S. Lewellen, Turbulent mixing with chemical reactions in the planetary boundary layer, *J. Appl. Meteorol.*, 33, 825–834, 1994.

Turner, B. J., M. Y. Leclerc, M. Gauthier, K. E. Moore, and D. R. Fitzjarrald, Identification of turbulence structures above a forest canopy using a wavlet transform, *J. Geophys. Res.*, 99, 1919–1926, 1994.

Verver, G., H. van Dop, and A. A. M. Holtslag, Turbulent mixing of reactive gases in the convective boundary layer, *Boundary-Layer Meteorol.*, 85, 197–222, 1997.

Vilà-Guerau de Arellano, J., and J. Lelieveld, Chemistry in the atmospheric boundary layer, in *Clear and Cloudy Boundary Layers*, edited by A. Holtslag and P. Duynkerke, pp. 267–286, KNAW, Amsterdam, Netherlands, 1998.

Vilà-Guerau de Arellano, J., P. G. Duynkerke, P. J. Jonker, and P. J. H. Builtjes, An observational study on the effects of time and space averaging in photochemical models, *Atmos. Environ.*, 27, 353–362, 1993.

M. C. Krol and M. J. Molemaker, Institute for Marine and Atmospheric Research, Utrecht, Princetonplein 5, 3584 CC, Utrecht, Netherlands. (krol@phys.uu.nl)

J. Vilà Guerau de Arellano, Department of Meteorology and Air Quality, Duivendaal 2, 6701 AP, Wageningen, Netherlands. (jvila@hp1.met.wau.nl)